The Twenty-Second International Symposium on Artificial Life and Robotics 2017 (AROB 22nd 2017),
The Second International Symposium on BioComplexity 2017 (ISBC 2nd 2017),
B-Con Plaza, Beppu, Japan, January 19-21, 2017

Analyses of Biped Walking Posture by Dynamical-Evaluating Index

Keli Shen[1], Xiang Li[1], Hongzhi Tian[1], Daiji Izawa[1] ,
Mamoru Minami [1]and Takayuki Matsuno[1]

[1]Okayama University, Japan
(Tel: 81-86-251-8233, Fax: 81-86-251-8233)
[1]pue85qr6@s.okayama-u.ac.jp

Abstract: In this paper, biped walking posture and design are evaluated through Dynamic Reconfiguration Manipulability Shape Index (DRMSI) which is the combination of dynamic manipulability and reconfiguration manipulability by using remaining redundancy. DRMSI represents how much the dynamical system of manipulators produces shape-changing acceleration ability in work space by normalized torque input, while the prior task is given to the hand motion. Besides, we use visual-lifting approach to enhance standing robustness and prevent the robot from falling down. In the application to the biped walking, the primary task is to keep the position of the head directing to the desired one as much as possible. And the second task is to realize the biped walking. Further, we confirm that the proposed analyses can be useful practically for evaluating the biped walking and biped humanoid robot has the optimal configuration to realize stable walking with more flexibility. Since this kinematic and dynamic characteristics are similar to human-being, our humanoid robot model is reliable and effective.

Keywords: DRMSI , Visual-lifting Approach, Humanoid, Biped walking, Height difference of ladder

1 INTRODUCTION

Many researchers made their efforts to control humanoid walking and proposed many effective methods to measure walking flexibility. It is known that ZMP-based walking motion is considered as the most effective and hopeful method, which has been proved to be an effective control way of performing stability of practical biped walking since it can ensure that the humanoid can achieve the balance of walking and standing by keeping the ZMP within the convex hull of supporting space [1]. Nakamura [2] showed connection between motions and environment by combining the dynamical equation of motion and put into execution on human. Since dimension number of biped walking dynamical states is varied by contacting conditions of foot with ground, we need some measurements to discuss continually kinematic and dynamical flexibility of humanoid according to the bipedal gaits' variety. The behavior of human's walking seems to use redundancy during performing a prior task of biped walking or eyes staring. Thus, we describe about dynamical redundancy of humanoid biped walking in this paper, and explain the concept of dynamical reconfiguration manipulability Shape Index (DRMSI), which can potentially produce a motion in a workspace with standardized input torque. Beside, DRM is combined by the dynamic manipulability (DM) [7] with reconfiguration manipulability (RM) [8]. The new index evaluates the flexibility of the dynamical system of humanoid robots. We have applied DRMSI to a humanoid robot, whose primary work is assigned to keep head position and orientation close to desired one as much as possible. The concept is shown in Fig. 1(b) and the Dynamic Reconfiguration Manipulability Ellipsoid (DRME) of floor-fixed four link robot is shown in Fig. 1(a). Simulations show that the value of DRME was relative to the change of the human's waist height, indicating that index can be useful such as the case that the whole shape-change control can be improved through DRME based on request of secondary work different from walking.

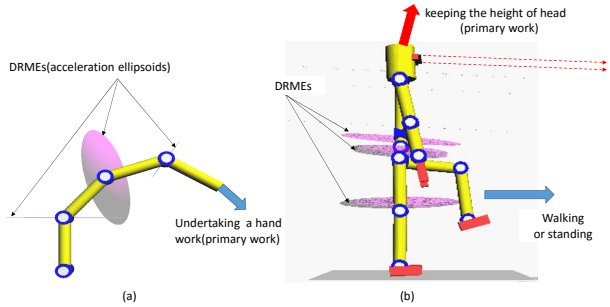

Fig. 1. Applications of DRME for (a) redundant manipulator and (b) humanoid robot.

Walking on the uneven floor is shown in Fig. 2. Considering condition of work-1 (keeping the height of head) and work-2 (lowering the height of waist) is set. These work give an assumption that humanoid's face and eyes should be targeted to certain object during walking on the uneven floor. There is space for z-acceleration of waist in (a), which enable robot to complete work-1 and work-2 simultaneously at the same time. However, there is little space for z-acceleration of waist in (b), work-1 can be completed but work-2 cannot be

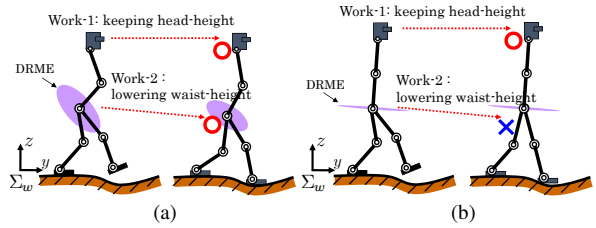

Fig. 2. Walking on uneven floor with (a) no-singular mechanics has a redundancy to accelerate the waist position during keeping head posture and making the foot reach the uneven floor (b) partially singular mechanics (from waist to head) has no ability to keep the current head posture, during the foot reaching floor. This result can be analyzed by the DRME , indicating the width in z-axis is nearly zero and ellipse shape is flat.

completed since head will go down when the foot approach floor. Therefore, DRMSI can be considered as an index to evaluate flexibility of plural work of biped walking. From our group simulation experiments, we find that humanoid robot similar to human-being is more suitable to walk on the even floor than to walk up and down the ladder, which is measured by the change of the DRMSI value. We will to use DRMSI to find out how to keep the highest flexibility of motion on the road with the uncertain and complexed condition such as stairs with different ladder heights or challenging terrain in the future.

2 DYNAMICAL BIPED WALKING MODEL

We discuss a humanoid robot described in Fig. 3. Table 1 shows length l_i [m], mass m_i [kg] of links and joints' coefficient of viscous friction d_i [N·m·s/rad], which are decided according to [3]. Our model figures rigid whole body—feet including toe, torso, arms and body—having 18 degree-of-freedom. Specific explanation of this model is skipped, which is mentioned in [4].

3 DYNAMIC RECONFIGURATION MANIPULABILITY

3.1 Dynamic Manipulability

In short, motion equation of serial link manipulators can be written as

$$\boldsymbol{M}(\boldsymbol{q})\ddot{\boldsymbol{q}}+\boldsymbol{h}(\boldsymbol{q},\dot{\boldsymbol{q}})+\boldsymbol{g}(\boldsymbol{q})+\boldsymbol{D}\dot{\boldsymbol{q}}=\boldsymbol{\tau} \tag{1}$$

where $\boldsymbol{M}(\boldsymbol{q}) \in R^{n\times n}$ represents inertia matrix, $\boldsymbol{h}(\boldsymbol{q},\dot{\boldsymbol{q}}) \in R^n$ and $\boldsymbol{g}(\boldsymbol{q}) \in R^n$ represent vectors of Coriolis force, centrifugal force and gravity, $\boldsymbol{D} = diag[d_1, d_2, \cdots, d_n]$ is matrix representing coefficients of joints' viscous friction and $\boldsymbol{\tau} \in R^n$ represents joint torque. The kinematic equation of manipulators, the relation between the j-th link's velocity $\dot{\boldsymbol{r}}_j \in R^m$ and the angular velocity $\dot{\boldsymbol{q}} \in R^n$ is described by

$$\dot{\boldsymbol{r}}_j = \boldsymbol{J}_j\dot{\boldsymbol{q}} \quad (j = 1,2,\cdots,n). \tag{2}$$

Then, $J_j \in R^{m\times n}$ can be described as Jacobian matrix including zero block matrix, $\boldsymbol{J}_j = [\tilde{\boldsymbol{J}}_j,\ \boldsymbol{0}]$. Through differentiating calculation of Eq.(2), we can achieve Eq.(3)

$$\ddot{\boldsymbol{r}}_j = \boldsymbol{J}_j(\boldsymbol{q})\ddot{\boldsymbol{q}}+\dot{\boldsymbol{J}}_j(\boldsymbol{q})\dot{\boldsymbol{q}} \tag{3}$$

where $\dot{\boldsymbol{J}}_j(\boldsymbol{q})\dot{\boldsymbol{q}}$ is the acceleration as Coliolis and centrifugal acceleration resulted from nonlinear relation of two-coordinates-space represented by $\boldsymbol{q}_i$ to $\boldsymbol{r}_i$. Then, we can obtain Eq.(4) from Eq.(1) and Eq.(3)

$$\ddot{\boldsymbol{r}}_j - \dot{\boldsymbol{J}}_j\dot{\boldsymbol{q}} = \boldsymbol{J}_j\boldsymbol{M}^{-1}[\boldsymbol{\tau}-\boldsymbol{h}(\boldsymbol{q},\dot{\boldsymbol{q}})-\boldsymbol{g}(\boldsymbol{q})-\boldsymbol{D}\dot{\boldsymbol{q}}]. \tag{4}$$

Here, two variables are defined as follows:

$$\tilde{\boldsymbol{\tau}} \triangleq \boldsymbol{\tau}-\boldsymbol{h}(\boldsymbol{q},\dot{\boldsymbol{q}})-\boldsymbol{g}(\boldsymbol{q})-\boldsymbol{D}\dot{\boldsymbol{q}}, \tag{5}$$

$$\ddot{\tilde{\boldsymbol{r}}}_j \triangleq \ddot{\boldsymbol{r}}_j - \dot{\boldsymbol{J}}_j\dot{\boldsymbol{q}} = \boldsymbol{J}_j\ddot{\boldsymbol{q}}. \tag{6}$$

Then, Eq.(4) can be rewritten as

$$\ddot{\tilde{\boldsymbol{r}}}_j = \boldsymbol{J}_j\boldsymbol{M}^{-1}\tilde{\boldsymbol{\tau}} \quad (j = 1,2,\cdots,n). \tag{7}$$

Considering serial desired accelerations $\ddot{\tilde{\boldsymbol{r}}}_j$ of all links being producible by serial joint torques $\tilde{\boldsymbol{\tau}}_j$ satisfying an Euclidean norm condition ($\|\tilde{\boldsymbol{\tau}}_j\| = (\tilde{\tau}_1^2+\tilde{\tau}_2^2+\cdots+\tilde{\tau}_j^2)^{1/2} \le 1$), and then the each tip acceleration makes an ellipsoid in range room of J_j. These ellipsoids of each link have been known as "Dynamic Manipulability Ellipsoid (DME) " from [7] (Fig. 4(a)) which are denoted in Eq.(8).

$$\ddot{\tilde{\boldsymbol{r}}}_j^T(\boldsymbol{J}_j(\boldsymbol{M}^T\boldsymbol{M})^{-1}\boldsymbol{J}_j^T)^+\ddot{\tilde{\boldsymbol{r}}}_j \le 1, \quad \textit{and} \quad \ddot{\tilde{\boldsymbol{r}}}_j \in R(\boldsymbol{J}_j) \tag{8}$$

where, $R(J_j)$ represents range room of J_j.

3.2 Dynamic Reconfiguration Manipulability

Here, the desired end-effector's acceleration $\ddot{\tilde{\boldsymbol{r}}}_{nd}$ is considered as prior work. Putting $j = n$ into Eq.(7), the desired $\ddot{\tilde{\boldsymbol{r}}}_j$ is described by $\ddot{\tilde{\boldsymbol{r}}}_{nd}$,

$$\ddot{\tilde{\boldsymbol{r}}}_{nd} = \boldsymbol{J}_n\boldsymbol{M}^{-1}\tilde{\boldsymbol{\tau}}. \tag{9}$$

From Eq.(9), $\tilde{\boldsymbol{\tau}}$ is obtained in (10)

$$\tilde{\boldsymbol{\tau}} = (\boldsymbol{J}_n\boldsymbol{M}^{-1})^+\ddot{\tilde{\boldsymbol{r}}}_{nd} + [\boldsymbol{I}_n-(\boldsymbol{J}_n\boldsymbol{M}^{-1})^+(\boldsymbol{J}_n\boldsymbol{M}^{-1})]\,{}^1\boldsymbol{l} \tag{10}$$

where, ${}^1\boldsymbol{l}$ represents an arbitrary vector which satisfies ${}^1\boldsymbol{l} \in R^n$. The left superscript "1" of ${}^1l$ represents the first dynamic configuration change subtask. In the right side of Eq.(10), the first part describes the solution of minimizing $\tilde{\boldsymbol{\tau}}$ in the null room of $\boldsymbol{J}_n\boldsymbol{M}^{-1}$ during executing $\ddot{\tilde{\boldsymbol{r}}}_{nd}$.

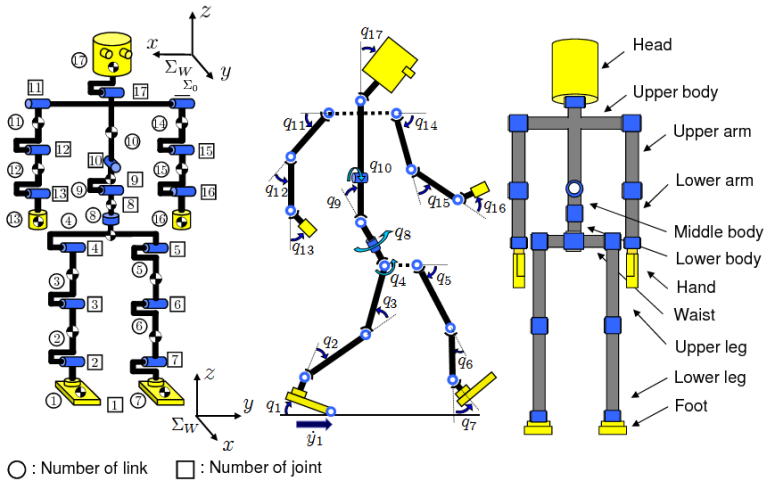

Fig. 3. Definition of humanoid's link, joint and angle number.

Table 1. Physical parameters.

Link	l_i	m_i	d_i
Head	0.24	4.5	0.5
Upper body	0.41	21.5	10.0
Middle body	0.1	2.0	10.0
Lower body	0.1	2.0	10.0
Upper arm	0.31	2.3	0.03
Lower arm	0.24	1.4	1.0
Hand	0.18	0.4	2.0
Waist	0.27	2.0	10.0
Upper leg	0.38	7.3	10.0
Lower leg	0.40	3.4	10.0
Foot	0.07	1.3	10.0
Total	1.7	64.2	

The second part describes the element of torques at each joint, which can change the configuration of manipulator despite of the influence of arbitrary $\ddot{\boldsymbol{r}}_{nd}$ as end-effector acceleration for trailing the desired path. In this research, ${}^1\ddot{\boldsymbol{r}}_{nd}$ is commanded by a higher-level dynamic reconfiguration control system and ${}^1\ddot{\boldsymbol{r}}_{jd}$ can be used for ordinary dynamic configuration change subtask. The relation between ${}^1\ddot{\boldsymbol{r}}_{jd}$ and $\ddot{\boldsymbol{r}}_{nd}$ is described in Eq.(11) by substituting Eq.(10) into ${}^1\ddot{\boldsymbol{r}}_{jd} = \boldsymbol{J}_j\boldsymbol{M}^{-1}\tilde{\boldsymbol{\tau}}$

$$
\begin{aligned}
{}^1\ddot{\boldsymbol{r}}_{jd} = {} & \boldsymbol{J}_j\boldsymbol{M}^{-1}(\boldsymbol{J}_n\boldsymbol{M}^{-1})^+\ddot{\boldsymbol{r}}_{nd} \\
& +\boldsymbol{J}_j\boldsymbol{M}^{-1}[\boldsymbol{I}_n-(\boldsymbol{J}_n\boldsymbol{M}^{-1})^+(\boldsymbol{J}_n\boldsymbol{M}^{-1})]\,{}^1\boldsymbol{l}. \quad (11)
\end{aligned}
$$

Here, two new variables are defined in the following equations

$$\Delta^1\ddot{\boldsymbol{r}}_{jd} \triangleq {}^1\ddot{\boldsymbol{r}}_{jd}-\boldsymbol{J}_j\boldsymbol{M}^{-1}(\boldsymbol{J}_n\boldsymbol{M}^{-1})^+\ddot{\boldsymbol{r}}_{nd}, \quad (12)$$

$${}^1\boldsymbol{\Lambda}_j \triangleq \boldsymbol{J}_j\boldsymbol{M}^{-1}[\boldsymbol{I}_n-(\boldsymbol{J}_n\boldsymbol{M}^{-1})^+(\boldsymbol{J}_n\boldsymbol{M}^{-1})]. \quad (13)$$

In Eq.(12), $\Delta^1\ddot{\boldsymbol{r}}_{jd}$ is named after "the first dynamic configuration change acceleration." In Eq.(13), ${}^1\Lambda_j$ is a $m\times n$ matrix named after "the first dynamic configuration change matrix." And then, Eq.(11) can be simplified as

$$\Delta^1\ddot{\boldsymbol{r}}_{jd} = {}^1\boldsymbol{\Lambda}_j\,{}^1\boldsymbol{l}. \quad (14)$$

The relation between ${}^1\ddot{\boldsymbol{r}}_{jd}$ and $\Delta^1\ddot{\boldsymbol{r}}_{jd}$ is shown in Fig. 5. However, the new problem is how to find out ${}^1l$ to generate $\Delta^1\ddot{\boldsymbol{r}}_{jd}$.
Solving ${}^1l$ in Eq.(14) as

$${}^1\boldsymbol{l} = {}^1\boldsymbol{\Lambda}_j^+\Delta^1\ddot{\boldsymbol{r}}_{jd}+(\boldsymbol{I}_n-{}^1\boldsymbol{\Lambda}_i^+\,{}^1\boldsymbol{\Lambda}_j)\,{}^2\boldsymbol{l}. \quad (15)$$

In Eq.(15), ${}^2l$ is an arbitrary vector which satisfies ${}^2l \in R^n$. ${}^1l$ is assumed to consist with restricted condition $\|{}^1l\| \le 1$, and

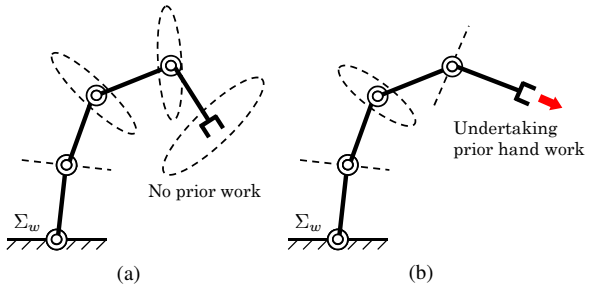

Fig. 4. (a) Dynamic manipulability ellipsoids (DMEs)(no prior work) and (b) dynamic reconfiguration manipulability ellipsoids (DRMEs) (undertaking prior work).

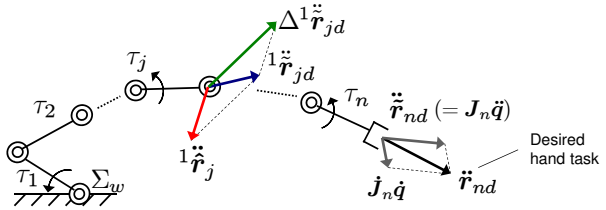

Fig. 5. Configuration change of intermediate links during manipulator executing work.

then next equation is obtained,

$$\Delta^1\ddot{\boldsymbol{r}}_{jd}{}^T({}^1\boldsymbol{\Lambda}_j^+)^T\,{}^1\boldsymbol{\Lambda}_j^+\Delta^1\ddot{\boldsymbol{r}}_{jd} \le 1. \quad (16)$$

If $rank({}^1\Lambda_i) = m$, Eq.(16) denotes an m-dimensional room ellipsoid, satisfying

$$\Delta^1\ddot{\boldsymbol{r}}_{jd} = {}^1\boldsymbol{\Lambda}_j\,{}^1\boldsymbol{\Lambda}_j^+\Delta^1\ddot{\boldsymbol{r}}_{jd}, \quad \Delta^1\ddot{\boldsymbol{r}}_{jd} \in R^m, \quad (17)$$

which means that $\Delta^1\ddot{\boldsymbol{r}}_{jd}$ can be arbitrarily obtained in m-dimensional room and Eq.(16) always has the value ${}^1l$ satisfying all $\Delta^1\ddot{\boldsymbol{r}}_{jd} \in R^m$. Besides, if $rank({}^1\Lambda_j) = a < m$, $\Delta\ddot{\boldsymbol{r}}_{jd}$ is not obtained arbitrarily in R^m. Thus, we name reduced $\Delta\ddot{\boldsymbol{r}}_{jd}$ after $\Delta^1\ddot{\boldsymbol{r}}^*_{jd}$. Then Eq.(16) can be denoted as the following equation, which is proposed by [9]

$$(\Delta^1\ddot{\boldsymbol{r}}^*_{jd})^T({}^1\boldsymbol{\Lambda}^+_j)^T\,{}^1\boldsymbol{\Lambda}^+_j\Delta^1\ddot{\boldsymbol{r}}^*_{jd} \leq 1$$
$$(\Delta^1\ddot{\boldsymbol{r}}^*_{jd} = {}^1\boldsymbol{\Lambda}_j\,{}^1\boldsymbol{\Lambda}^+_j\Delta^1\ddot{\boldsymbol{r}}_{jd}). \tag{18}$$

Equation (18) denotes an a-dimensional room ellipsoid. These ellipsoid described in Eq.(16) and Eq.(18) are shown in Fig.4(b). Therefore, if the matrix $\boldsymbol{\Lambda}$ is conducted by the singular value dissolution, we can get

$${}^1\boldsymbol{\Lambda}_j = {}^1\boldsymbol{U}_j\,{}^1\boldsymbol{\Sigma}_j\,{}^1\boldsymbol{V}_j^T \tag{19}$$

$${}^1\boldsymbol{\Sigma}_i = \begin{array}{c} \\ a \\ m-a \end{array} \begin{array}{c} \begin{array}{ccc} a & & n-a \end{array} \\ \begin{bmatrix} {}^1\sigma_{j,1} & & \boldsymbol{0} \\ & \ddots & & \boldsymbol{0} \\ \boldsymbol{0} & & {}^1\sigma_{j,a} \\ & \boldsymbol{0} & & \boldsymbol{0} \end{bmatrix} \end{array}. \tag{20}$$

In Eq.(19) and Eq.(20), ${}^1\boldsymbol{U} \in R^{m\times m}$, ${}^1\boldsymbol{V} \in R^{n\times n}$ denote orthogonal matrixes, and a is the number of non-zero singular values of ${}^1\boldsymbol{\Lambda}_j$ ($\sigma_{j,1} \geq \cdots \geq \sigma_{j,a} > 0$). Besides, $a \leq m$ since $rank({}^1\boldsymbol{\Lambda}_j) \leq m$. Thus, when the end-effector of manipulator executes some work, dynamic configuration change flexibility of j-th link can be denoted as

$${}^1w_j = {}^1\sigma_{j,1} \cdot {}^1\sigma_{j,2} \cdots {}^1\sigma_{j,a}. \tag{21}$$

In this paper, we name the value of w_j in Eq.(21) after dynamic reconfiguration manipulability measure (DRMM), indicating the degree of that configuration change acceleration of j-th link can be obtained from different direction. And then, volume of dynamic configuration change ellipsoid at the j-th link is defined as

$${}^1V_{DRj} = c_m \cdot {}^1w_j \tag{22}$$

$$c_m = \begin{cases} 2(2\pi)^{(m-1)/2}/[1\cdot 3\cdots(m-2)m] & (m:odd) \\ (2\pi)^{m/2}/[2\cdot 4\cdots(m-2)m] & (m:even) \end{cases}. \tag{23}$$

For taking dynamic reconfiguration measure of the whole manipulator-links into consideration, we give an indicatrix called dynamic reconfiguration manipulability shape index (DRMSI):

$${}^1W_{DR} = \sum_{j=1}^{n-1} a_j\,{}^1V_{DRj}. \tag{24}$$

In this paper, singular-values are enlarged a hundredfold to obtain formal value of ellipsoid, comparing with ellipse or line segment. For robots in sagital plane like Fig. 4(b), a_j is denoted as

$$a_1 = a_{n-1} = 1[m^{-1}],\ a_{2,3,\cdots,(n-2)} = 1[m^{-2}]. \tag{25}$$

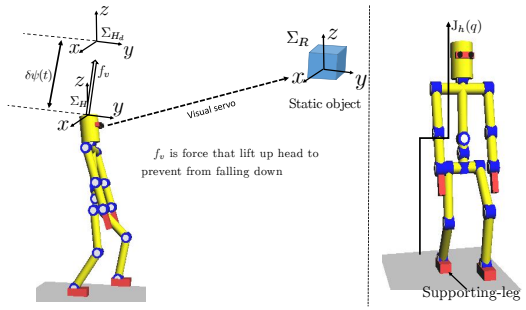

Fig. 6. Concept of Visual Lifting Stabilization.

4 VISUAL LIFTING METHOD

This section proposes a vision-feedback control to strengthen biped standing/walking stability as shown in Fig. 6. We apply visual servoing method to evaluate posture of a static target object described by $\psi(t)$ representing the robot's head based on Σ_H. The relatively desired posture of Σ_R (coordinate of reference target object) and Σ_H is predefined by Homogeneous Transformation as ${}^H\boldsymbol{T}_R$. The difference of the desired head posture Σ_{H_d} and the current posture Σ_H is defined as ${}^H\boldsymbol{T}_{H_d}$, it can be described by

$${}^H\boldsymbol{T}_{H_d}(\psi_d(t),\psi(t)) = {}^H\boldsymbol{T}_R(\psi(t)) \cdot {}^{H_d}\boldsymbol{T}_R{}^{-1}(\psi_d(t)), \tag{26}$$

where ${}^H\boldsymbol{T}_R$ is calculated by $\psi(t)$ that can be measured by on-line visual posture evaluate approach, which is proposed by [5], [6]. However, in this paper, we assume that this parameter is given directly. Here, the force which is exerted on the head to minimize $\delta\psi(t)(=\psi_d(t)-\psi(t))$ calculated from ${}^H\boldsymbol{T}_{H_d}$ is considered to be directly proportional to $\delta\psi(t)$. The deviation of the robot's head posture is caused by gravity force and the influence of walking dynamics. The joint torque $\boldsymbol{\tau}_h(t)$ lifting the robot's head is given as the following equation:

$$\boldsymbol{\tau}_h(t) = \boldsymbol{J}_h(\boldsymbol{q})^T\boldsymbol{K}_p\delta\psi(t) \tag{27}$$

where $\boldsymbol{J}_h(\boldsymbol{q})$ in Fig. 6 is Jacobian matrix of the head posture against joint angles including $q_1, q_2, q_3, q_4, q_8, q_9, q_{10}$ and q_{17}, also $\boldsymbol{K}_p$ is proportional gain like impedance control. We apply this input to prohibit the behavior of falling down caused by gravity or dangerous slipping gaits happened unpredictably during walking progress. $\delta\psi(t)$ can show the deviation of the humanoid's position and orientation, however, only position was discussed in this study.

5 APPLICATION TO HUMANOID BIPED ROBOT BASED ON DRMSI

This section is aimed at using the measurement tool to analyze the flexibility of biped walking. The robot head is kept in constant height and we assume the constraint condition $\|{}^1\,l\,\| \leq 1$. DRMEs of humanoid robot are plotted in Fig. 7.

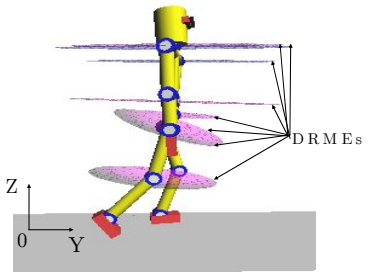

Fig. 7. The DRMEs of biped walking humanoid

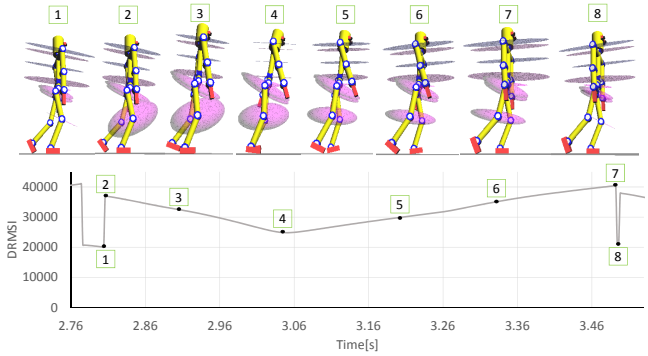

Fig. 8. Screen-shot of walking states corresponding to DRMSI from 2.76[s] to 3.53[s].

There are 8 ellipses generating on the tip of the links. The volume of ellipse is formed by the manipulability to investigate the acceleration performance of biped walking links. Here, DRMEs are determined by ${}^1\boldsymbol{\Lambda}_j$, which depends on both the jacobian matrix and the inertial matrix in Eq.(13). Furthermore, two variables mentioned above are theoretically the functions of joint angles from the supporting foot to the head. Therefore, DRMEs are theoretically dominated by joint angles. In other words, DRMEs are determined by the configuration of biped walking robot. Combining the shape of ellipse in Fig. 7 and Eqs.(20), (21), (22), we can find that ellipse area is composed of the lines representing the all the accelerations produced in the different directions of whole or part workspace. In Eq.(20), ${}^1\sigma_{j,1}$,${}^1\sigma_{j,2}$ correspond to the major axis and minor axis, representing the biggest acceleration and the smallest acceleration. And then, we calculate all the joint reconfiguration flexibility with Eq.(24) from the supporting foot to the head except the head ellipsoid since keeping the height of the head is prior task. The value of DRMSI is the total of the calculated joint acceleration while obtaining the optimal walking configuration by adjusting the joint angles.

Then, biped walking is simulated on the even ground. In this simulation, we set three sorts of lifting-proportional-gain

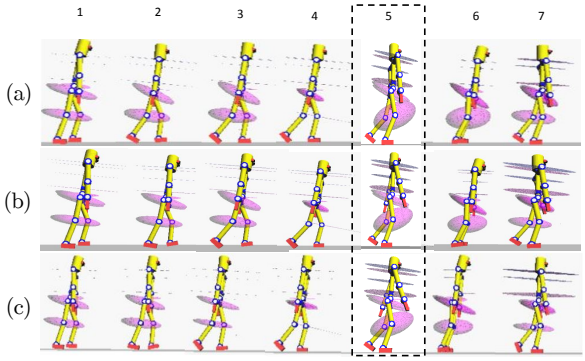

Fig. 9. Screen-shot of biped walking with DRMEs about different gain set : (a) $\boldsymbol{K}_p = diag[20,290,1000]$, (b) $\boldsymbol{K}_p = diag[20,290,1050]$, (c) $\boldsymbol{K}_p = diag[20,290,1100]$.

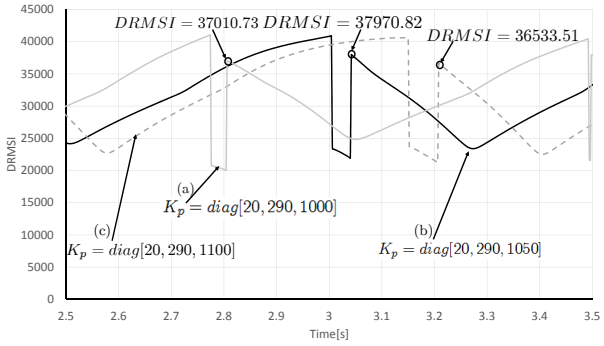

Fig. 10. DRMSI when t is from2.5$[s]$ to 3.5$[s]$.

in Eq.(27), such as $(a)\boldsymbol{K}_p = diag[20,290,1000]$, $(b)\boldsymbol{K}_p = diag[20,290,1050]$ and $(c)\boldsymbol{K}_p = diag[20,290,1100]$, to analyze that how the different heights of waist influence the biped walking flexibility and stability according to comparing the DRMSI values corresponding to different walking gaits. Besides, there are 8 kinds of walking states corresponding to DRMSI from 2.76[s] to 3.53[s] in Fig. 8, which indicates that DRMSI changes according to the configuration of humanoid robot. Thus, we choose the states that supporting-foot keeps surface-contact, which was easy to obtain and compare DRMSI shown in Fig. 9 (a)-5, (b)-5, (c)-5. In Fig. 10, the marked point means DRMSI obtained while the gaits is like (a)-5, (b)-5, (c)-5. Comparing the value, we get a conclusion that as the lifting gain become larger keeping the stable walking, DRMSI of (b)-5 is larger than others, which means there is an optimal configuration to keep better walking flexibility.

Furthermore, in Fig. 11, the trajectory is designed to estimate the DRM of humanoid walking on the ladder. Besides, height difference of ladder δh was set as 0.02[m],0.04[m] to consider the influence on biped walking humanoid con-

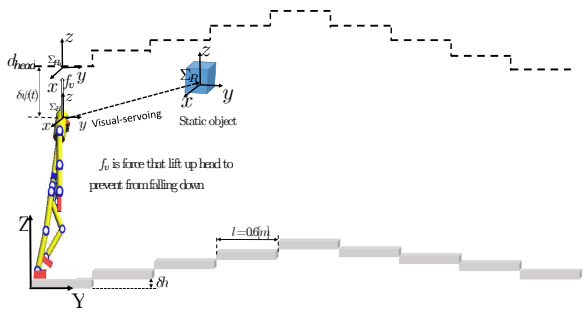

Fig. 11. humanoid walking on the ladder

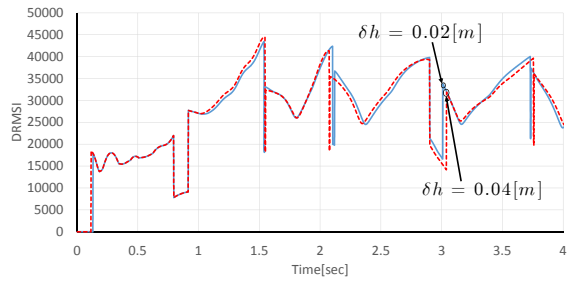

Fig. 12. DRMSI until $t = 4.0[s]$,$\boldsymbol{K}_p = diag[20, 290, 1050]$

figuration. The gain $\boldsymbol{K}_p = diag[20, 290, 1050]$, which enables humanoid robot to walk stably, were chosen to evaluate the influence of the change of height difference of ladder on DRMSI. The value change of DRMSI was shown in Fig. 12. In the case that humanoid robot walked on the ladder with lifting-gain $\boldsymbol{K}_p = diag[20, 290, 1050]$, if the height difference of ladder increased, the value of DRMSI when humanoid robot walked up and down the step became smaller, which was shown in Fig. 12. In other words, humanoid robot can walk more stably and faster on even ground than on the ladder.

6 CONCLUSION

In this paper, we explained DRMSI for the optimization of dynamic flexibility using redundancy for reconfiguration. And DRMSI was applied to our simulation experiments of humanoid biped walking. According to changing the waist height and ladder height difference, we found that walking flexibility and stability were different by the value of DRMSI, which indicated that our robot model was similar to human-being on the kinematic and dynamic characteristics such as suitable walking posture. On the other hand, we demonstrated that our new humanoid robot model was correct and effective.

REFERENCES

[1] M. Vukobratovic, A. Frank and D. Juricic, “On the Stability of Biped Locomotion,” *IEEE Transactions on Biomedical Engineering*, Vol. 17, No. 1, 1970.

[2] Y. Nakamura and K. Yamane, “Dynamics of Kinematic Chains with Discontinuous Changes of Constraints—Application to Human Figures that Move in Contact with the Environments,” *Journal of RSJ*, Vol. 18, No. 3, pp. 435–443, 2000 (in Japanese).

[3] M. Kouchi, M. Mochimaru, H. Iwasawa and S. Mitani, “Anthropometric database for Japanese Population 1997-98,” Japanese Industrial Standards Center (AIST, MITI), 2000.

[4] T. Maeba, M. Minami, A. Yanou, J. Nishiguchi, “Dynamical Analyses of Humanoid’s Walking by Visual Lifting Stabilization Based in Event-driven State Transition Cooperative manipulations based on Genetic Algorithms using contact information,” *2012 IEEE/ASME Int. Conf. on Advanced Intelligent Mechatronics Proc.*, pp. 7–14, 2012.

[5] W. Song, M. Minami, F. Yu, Y. Zhang and A. Yanou, “3-D Hand & Eye-Vergence Approaching Visual Servoing with Lyapunov-Stable Pose Tracking,” *Proceedings of IEEE International Conference on Robotics and Automation*, pp. 5210–5217, 2011.

[6] F. Yu, W. Song and M. Minami, “Visual Servoing with Quick Eye-Vergence to Enhance Trackability and Stability,” *Proceedings of IEEE/RSJ International Conference on Intelligent Robots and Systems*, pp. 6228–6233, 2010.

[7] T. Yoshikawa, “Dynamic Manipulability of Robot Manipulators,” *Proceedings of the IEEE International Conference on Robotics and Automation*, Vol. 2, No. 1, pp. 113–124, 1985.

[8] M. Minami, Y. Naitoh and T. Asakura, “Avoidance Manipulability for Redundant Manipulators,” *Journal of the Robotics Society of Japan*, Vol. 17, No. 6, pp. 887–895, 1999 (in Japanese).

[9] M. Minami, X. Li, T. Matsuno and A. Yanou, “Dynamic Reconfiguration Manipulability for Redundant Manipulators,” *Journal of the Mechanisms Robotics* , Vol. 8 / 061004-1-061004-9, 2016.

[10] Y. Kobayashi, M. Minami, A. Yanou and T. Maeba “Dynamic Reconfiguration Manipulability Analyses of Humanoid Bipedal Walking,” *Proceedings of the IEEE International Conference on Robotics and Automation (ICRA),* , pp. 4764-4769, 2013.